Spectroscopic Investigation of Artificial Opals Infiltrated with a Heteroaromatic Quadrupolar Dye

Luca Berti, Marco Cucini, Francesco Di Stasio,[†] and Davide Comoretto*

Dipartimento di Chimica e Chimica Industriale, Università degli Studi di Genova, via Dodecaneso 31, I-16146 Genova, Italy

Matteo Galli and Franco Marabelli

Dipartimento di Fisica "A. Volta", Università degli Studi di Pavia, via Bassi 6, 27100 Pavia, Italy

Norberto Manfredi, Chiara Marinzi, and Alessandro Abbotto*

Dipartimento di Scienza dei Materiali e INSTM, Università degli Studi di Milano-Bicocca, Via Cozzi 53, I-20125, Milano, Italy

Received: June 26, 2009; Revised Manuscript Received: November 23, 2009

We report on the optical properties of polystyrene opals infiltrated with solutions of ad hoc synthesized heteroaromatic quadrupolar dyes endowed with strong nonlinear optical properties (two-photon absorption). Transmittance spectroscopy of opals infiltrated with dye water solutions shows both a bathochromic shift and a reduced width of the photonic crystal stop band. Moreover, variable angle transmittance spectra highlight the high energy dispersion of the stop band upon increasing the incidence angle. Photoluminescence spectra recorded at different emission angles with respect to the normal of the sample for such infiltrated opals show that the emission spectrum is strongly modified at the stop band according to the opal dispersion properties. A careful comparison of the intensity and spectral properties of photoluminescence in opals possessing a properly tuned photonic stop band is reported and discussed. Two different effects are observed: when concentrated solutions are used, emitted light filtering due to the photonic stop band is observed. On the other hand, by properly reducing solution self-absorption, directional enhancement of emission in the high energy side of the stop band is observed. Physical mechanisms responsible for this phenomenon are discussed.

1. Introduction

Among photonic crystals (PhC), i.e., materials possessing a periodic modulation of the dielectric constant on a length scale comparable to the wavelength of visible light,[1,2] artificial opals are a simple, cheap, and interesting playground to investigate optical effects on this class of nanostructured materials. Despite the fact that opals do not show a complete photonic band gap (PBG) but only a pseudogap (stop band),[3] their versatility allows interesting structures to be obtained. As a matter of fact, they can be employed as templates to prepare inverse opals (which instead might have a complete PBG[4]), they can be engineered with structural defects,[5] and they can also be infiltrated with a variety of materials ranging from metals to organic semiconductors.[6] A large amount of work on opal infiltration has been done in the last years (see, for instance, the review in ref 6), and the proper choice of the infiltrating material allows the optical properties of the PhC to be tailored for selected applications. Among all possible materials used for opal infiltration, we focused our interest on molecular semiconductors, whose optical and electronic properties can be chemically tailored for specific functions. Opals infiltrated with highly efficient nonlinear molecular emitters showed unusual effects on two-photon excited emission spectra when the chromophore emission was properly tuned within the stop band of the opal.[7] Moreover, a dramatic enhancement of the third harmonic generation efficiency was observed when phase matching conditions were provided by the periodical structure of the opal photonic crystal.[8] Artificial opals infiltrated with π-conjugated polymers exhibit random lasing action. With such a system, simultaneous laser emission of different colors has also been demonstrated.[9,10] Photonic crystal polaritons have also been observed in opals possessing the stop band properly tuned with the sharp and strong absorption of excitons both in molecular J-aggregates[11] or pervoskites.[12] Moreover, energy transfer, emission enhancement, and other fine effects caused by the photonic structure on the emission properties of dye or quantum dots have also been reported.[13–28] In general, we notice that the dyes used in those papers are either commercially available species with the absence of engineered properties or well-known systems used to probe a specific optical effect. Not much effort has been so far dedicated to investigating and to characterizing novel dyes with peculiar and tailored properties when infiltrated inside a photonic crystal structure.

In this work, we report on the results of a wide spectroscopic characterization of opal infiltrated with solutions of quadrupolar dyes derived from PEPEP molecule (dye **1** in Figure 1). The reason for our interest in PEPEP derivatives is related to their large two-photon absorption (TPA) properties.[29] The two-photon absorption phenomenon has been used in conventional and

* To whom correspondence should be addressed. E-mail: comorett@chimica.unige.it (D.C.); alessandro.abbotto@mater.unimib.it (A.A.). Phone: +39-0103538736 (D.C.); +39-0264485227 (A.A.). Fax: +39-0103538733 (D.C.); +39-0264485400 (A.A.).

† Current address: Department of Physics and Astronomy and London Centre for Nanotechnology, University College London, London, WC1E 6BT, United Kingdom.

10.1021/jp906002q
Published on Web 01/22/2010

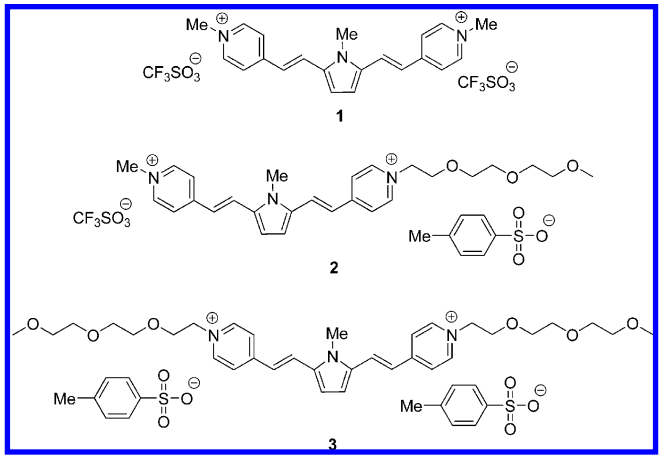

Figure 1. Chemical structure of PEPEP (**1**), monoTEG-PEPEP (**2**), and bisTEG-PEPEP (**3**).

emerging photonic and biomedical technologies[30] such as two-photon laser scanning fluorescence microscopy[31–33] and ion sensing,[34] photodynamic therapy,[35–37] optical limiting,[38,39] holographic recording and photorefractive effect,[40] microfabrication,[41] telecommunications,[42] and upconverted lasing.[43–45]

These nonlinear optical properties stem from the A-π-D-π-A general quadrupolar framework of the PEPEP molecule, where A is a pyridinium π-deficient heteroaromatic ring (electron acceptor) and D a π-excessive pyrrolyl moiety (electron donor) connected through a π-conjugated segment. The fluorescence quantum yield is 0.14 and the TPA cross section (σ_{TPA}) at 790 nm was measured to be 119 GM (*Z*-scan measurements, 150 fs pulses). More recently, two-photon induced fluorescence studies have shown σ_{TPA} values in the 100−800 GM range, with a maximum at about 820 nm.[29] These properties make PEPEP derivatives very interesting for PhC applications. However, before investigating the nonlinear optical properties of these dyes infiltrated in PhC, a linear optical characterization is a prerequisite to check chemical compatibility and basic physical properties.

In order to obtain polystyrene opals infiltrated with the heteroaromatic TPA quadrupolar dye **1**, solutions of the chromophore in water or other nonsolvents for polystyrene need to be used. We have therefore envisaged the new PEPEP derivatives **2** (monoTEG-PEPEP) and **3** (bisTEG-PEPEP) where one and two tris(ethylene glycol) monomethyl ether (TEG) chains, respectively, were introduced onto the terminal pyridinium moieties in order to impart solubility in hydrophilic and other polar solvents (Figure 1).

Preliminary data have shown that infiltration of polystyrene opals with solutions of dyes **2** and **3** in water is possible.[47] Here, we extend the investigation to the dispersion properties of photoluminescence spectra as well as to the effect of photonic band structure on spectral redistribution of emission intensity. To this end, different PL intensity references are used. Moreover, the role of solution concentration on PL self-absorption and PL directional enhancement is discussed.

2. Experimental Section

2.1. Chromophores Synthesis. ^{1}H and ^{13}C NMR spectra were recorded using a Bruker AMX-500 spectrometer operating at 500 and 125.70 MHz, respectively. Coupling constants are presented in hertz. Microwave irradiated reactions were performed with a CEM Discover Labmate reactor. Reagents and solvents were supplied by Aldrich. Dry acetone was stored over $CaCl_2$.

MonoTEG-PEPEP (2). A solution of **4** (0.280 g, 0.620 mmol) and TEG *p*-toluenesulfonate (TEG tosylate, TEG-OTs) (0.200 g, 0.628 mmol) in dry acetone (4 mL) was irradiated at a constant power of 90 W in a microwave reactor for 3 h. After cooling to room temperature, the dark precipitate was isolated by filtration and washed with cold acetone and toluene to afford the product **2** (0.455 g, 0.591 mmol, 94%). ^{1}H NMR (DMSO-d_6): δ 8.79 (2H, d, J = 6.9), 8.76 (2H, d, J = 6.9), 8.20 (2H, d, J = 6.8), 8.18 (2H, d, J = 6.8), 8.03 (1H, d, J = 15.8), 8.02 (1H, d, J = 15.8), 7.49 (2H, d, J = 8.0), 7.32 (1H, d, J = 15.8), 7.31 (1H, d, J = 15.8), 7.15−7.09 (4H, m), 4.64 (2H, t, J = 4.7), 4.22 (3H, s), 3.97 (3H, s), 3.90 (2H, t, J = 4.9), 3.59−3.54 (2H, m), 3.50−3.44 (4H, m), 3.43−3.38 (2H, m), 3.23 (3H, s), 2.29 (3H, s). ^{13}C NMR (DMSO-d_6): δ 153.5 (*C*), 152.9 (*C*), 146.4 (*C*), 145.0 (2C, *C*H), 144.6 (2C, *C*H), 138.0 (*C*), 136.2 (*C*), 136.0 (*C*), 128.9 (*C*H), 128.5 (*C*H), 128.5 (2C, *C*H), 125.9 (2C, *C*H), 123.2 (2C, *C*H), 123.1 (2C, *C*H), 121.8 (*C*H), 121.6 (*C*H), 114.1 (*C*H), 114.0 (*C*H), 71.7 (*C*H$_2$), 70.2 (*C*H$_2$), 70.0 (2C, *C*H$_2$), 69.2 (*C*H$_2$), 59.4 (*C*H$_2$), 58.6 (*C*H$_3$), 47.0 (*C*H$_3$), 31.3 (*C*H$_3$), 21.2 (*C*H$_3$). HRMS-ESI: *m*/*z* calcd for [M-CF_3SO_3-TsO]$^{2+}$ 449.26674/2 = 224.63337, found 224.63332; calcd for [M-TsO]$^+$ 598.21932, found 598.21940.

BisTEG-PEPEP (3). A solution of **5**[24] (0.050 g, 0.174 mmol) and TEG-OTs (0.450 g, 1.41 mmol) in dry acetone (6 mL) was irradiated at a constant power of 100 W in a microwave reactor for 3 h. Toluene (4 mL) was added, and the obtained dark precipitate was isolated and washed several times with toluene and petroleum ether. Crystallization from acetone afforded the pure product as a dark purple solid (0.119 g, 0.129 mmol, 74%). ^{1}H NMR (DMSO-d_6): δ 8.78 (4H, d, J = 6.6), 8.20 (4H, d, J = 6.6), 8.04 (2H, d, J = 15.8), 7.50 (4H, d, J = 7.9), 7.33 (2H, d, J = 15.8), 7.14 (2H, s), 7.12 (4H, d, J = 7.9), 4.64 (4H, t, J = 4.4), 3.97 (3H, s), 3.90 (4H, t, J = 4.2), 3.57 (4H, t, J = 4.0), 3.50−3.43 (8H, m), 3.43−3.38 (4H, m), 3.23 (6H, s), 2.28 (6H, s). ^{13}C NMR (DMSO-d_6): δ 153.5 (2C, *C*), 146.3 (2C, *C*), 144.6 (4C, *C*H), 138.0 (2C, *C*), 136.2 (2C, *C*), 128.9 (2C, *C*H), 128.5 (4C, *C*H), 126.0 (4C, *C*H), 123.1 (4C, *C*H), 121.7 (2C, *C*H), 114.2(2C, *C*H), 71.7 (2C, *C*H$_2$), 70.2 (2C, *C*H$_2$), 70.0 (4C, *C*H$_2$), 69.2 (2C, *C*H$_2$), 59.4 (2C, *C*H$_2$), 58.5 (2C, *C*H$_3$), 31.4 (*C*H$_3$), 21.2 (2C, *C*H$_3$). HRMS-ESI: *m*/*z* calcd for [M-2TsO]$^{2+}$ 581.34539/2 = 290.67269, found 290.67235.

2.2. Opals and Chromophore Infiltrated Opals. Commercial polystyrene monodisperse microsphere (diameter a = 222, 240, 260, and 300 nm; refractive index n_{PS} = 1.59; standard deviation <5%) water suspensions, 10% in volume (Duke Scientific), were used for opal preparation. In order to have a suitable sample thickness (d), we properly diluted these suspensions with deionized water and then we grew opal films by using the meniscus technique. Growth occurred at 45 ± 1 °C inside a BF53 Binder incubator. Opals were composed of flat domains with the [111] direction of the face centered cubic lattice of spheres perpendicular to the substrate. In better samples used for this work, domain sizes are 50−100 μm. However, defects inside these domains cannot be excluded. Further details including scanning electron images of similar samples can be found in refs 48–52.

Glass substrates coated with opal films having an area of ~7 × 7 mm^2 were sandwiched to an optical glass window through a spacer, thus forming a cell which was filled with water dye solutions. The spacer thickness was adjusted to be as similar as possible to the opal thickness in order to remove effects from free solution. In a few seconds, the solution spontaneously infiltrated the interstices between the microspheres. We used samples having different thicknesses; only for thinner ones it

TABLE 1: Sphere Diameter, Interplanar Spacing along the 111 direction (D), Stop Band Position (E_B), Standard Deviation of E_B, Stop Band Full Width at Half-Maximum (ΔE_B), Its Standard Deviation, $\Delta E_B/E_B$, L_B, Opal Thickness (d), and Correspondent Number of Sphere Layers for Bare and Infiltrated Opals Used in This Work as Determined by Transmittance and Reflectance Spectra[a]

	sphere diameter (nm)	D (nm)	E_B (cm^{-1})	$\sigma(E_B)$	ΔE_B (cm^{-1})	$\sigma(\Delta E_B)$	$\Delta E_B/E_B$	L_B (μm)	d (μm)	layers
$\langle R\rangle$ bare	222	181.26	19667.70	62.9	1355.80	11.46	0.07	1.7		
$\langle T\rangle$ bare	222	181.26	19739.40		2127.50		0.11	1.1		
$\langle T\rangle$ infiltrated	222	181.26	18698.60							
$\langle R\rangle$ bare	240	195.96	17771.31	293.3	1125.34	101.50	0.06	2.0		
$\langle T\rangle$ bare	240	195.96	17787.30		1698.90		0.10	1.3		
T infiltrated	240	195.96	17088.20		348.00		0.02	6.1	6.3	32
$\langle R\rangle$ bare	260	212.29	17236.95	6.3	1157.20	13.86	0.07	2.0		
$\langle T\rangle$ bare	260	212.29	17021.30		1358.80		0.08	1.7		
T infiltrated 1	260	212.29	15918.50		668.90		0.04	3.2	5.7	27
T infiltrated 2	260	212.29	16041.02		690.43		0.04	3.1	8.2	38
$\langle R\rangle$ bare	300	244.95	14833.96	71.4	943.70	30.62	0.06	2.5		
$\langle T\rangle$ bare	300	244.95	14768.87		1302.50		0.09	1.8		
T infiltrated 1	300	244.95	13706.10		657.50		0.05	3.3	12.5	51
T new infiltrated 2	300	244.95	13942.38		588.74		0.04	3.7	8.4	34

[a] For bare opals, we report the average data from R and T spectra. For infiltrated samples, we report (when possible) data for samples whose opal thickness was determined.

was possible to estimate d from the interference fringes in optical spectra (more than 6 μm thick; see Table 1 for details). Sample uniformity is quite good as determined by the reduced standard deviation of the stop band position in the optical data (Table 1). We tested 16 cells with 260 nm opals; 2 cells for 222 nm opals, 2 cells for 240 nm opals, and 2 cells for 300 nm opals were used as references.

2.3. Spectroscopy. Transmittance (T) and photoluminescence (PL) spectra were measured with optical setups based on an Avantes 2048 compact fiber optic spectrometer working in the range 250−1100 nm with a resolution of ~1.5 nm. The sample was mounted on a rotating stage allowing for T measurements at different incidence angles (θ) in the range 0−60°. The collimated white light probing beam has a diameter of 0.5 mm. All PL measurements were performed in backscattering geometry with the same setup recording emitted light coming out from the substrate side. This configuration prevents possible emission from molecules lying on the opal surface. For angle resolved PL measurements, the collection optics was kept fixed, whereas the sample was rotated an angle θ' with respect to it. The excitation for PL spectra was provided by a 405 nm Oxxius (model 405-50-COL-PP) laser diode having 50 mW as a maximum power. The collimated laser beam, 2 mm diameter, excites the sample with an estimated power of <10 mW. The incidence angle with respect to the optical system axis is fixed to about 30°. Then, the absolute intensity of the exciting beam depends on the rotating angle. However, since reference spectra are collected with the same setup in the same conditions, these effects cancel out during normalization. The numerical aperture of the collecting optics can be estimated by the iris diaphragm in front of the collecting lens (0.5−5 mm) and the distance between the sample and lens (50 mm) as NA ~ $1/(2F_{number})$ = 0.005−0.05. Light from the iris is then focused on an optical fiber (diameter 600 μm, NA = 0.2) and goes directly to the spectrophotometer having a 25 μm wide entrance slit. A scheme of the optical setup is available online as Supporting Information.

Particular care was paid in order to evaluate the angular-dependent PL enhancement. Solution infiltrated opals having a stop band fully detuned with respect to bisTEG-PEPEP photoluminescence (PL) spectra were used as a reference in order to reveal angular-dependent intensity enhancement effects. Notice that free solutions are not suitable for comparison of the absolute PL intensity, since light extraction from the cells is governed by the refractive index variation at the infiltrated opal/glass interface which is noticeably different from that found at the free solution/glass interface.

SCHEME 1: Synthesis of monoTEG-PEPEP and bisTEG-PEPEP

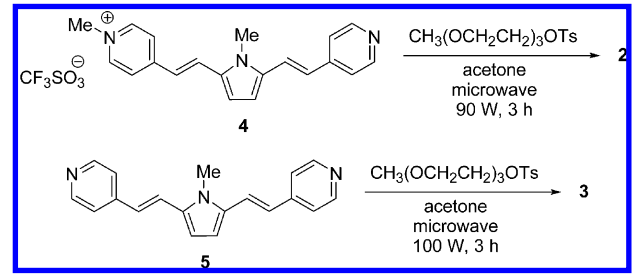

3. Results and Discussion

3.1. Synthesis and Linear Optical Properties of Hydrophilic Quadrupolar Chromophores. The two hydrophilic dyes **2** and **3** were synthesized according to Scheme 1. The monoTEG derivative **2** was obtained in 94% yield by alkylation of the monopyridinium precursor **4**[53,54] with TEG-OTs[55] in acetone in a microwave reactor. The same reaction can be carried out in CH_3CN in good yields (85%), but in this case, the isolation of the product is harder due to its large solubility in the reaction solvent. It is worth noting that the same reaction in acetone or CH_3CN at reflux without the use of the microwave irradiation did not lead to any formation of the product. The bisTEG derivative **3** was obtained in good yields (74%) in a similar manner by alkylation of the bidentate precursor **5**[54] with TEG-OTs in a microwave reactor.

As expected, the absorption spectra of the hydrosoluble dyes **2** and **3** are similar to that of the parent chromophore **1** in DMSO solution. The absorption and emission maxima of **1** in DMSO are 524 and 620 nm, respectively.[29,46] BisTEG-PEPEP shows an absorption peak at 526 nm in DMSO while PL maximum is slightly shifted to 609 nm, independently of the excitation wavelength (λ_{exc} = 405, 470, and 525 nm).[47] When the derivative **3** is dissolved in water, that is, the solvent used for opal infiltration, a more significant variation is observed with absorption and emission peaks at 507 and 598 nm, respectively (Figure 2).

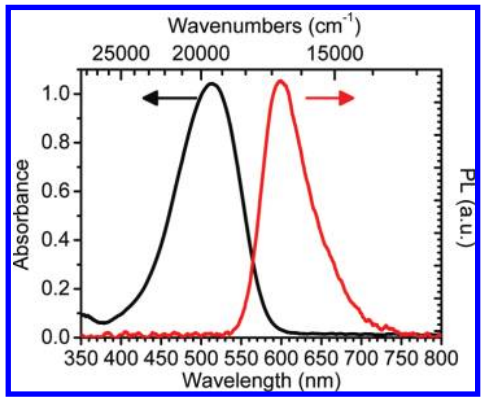

Figure 2. Absorption and PL spectra of chromophore **3** in water.

3.2. Optical Properties of Bare and Infiltrated Opals. We succeeded in opal infiltration with both dyes **2** and **3**. However, only data relative to dye **3** are here presented and discussed, since the presence of two hydrophilic TEG chains in place of one makes its solubility in water superior. No significant differences in the optical properties of opals infiltrated with solutions of the two molecules are observed.

Transmission spectra at normal incidence for bare and dye **3** solutions (1.4×10^{-3} M) infiltrated opals made by spheres having different diameters are shown in Figure 3. These spectra are compared to those for bare opals as well as to photoluminescence spectra of bisTEG-PEPEP water solutions. The sphere diameter determines the length of the face centered cubic cell ($l = a(2)^{0.5}$) and the spacing between sphere layers ($D = a(2/3)^{0.5}$) and, consequently, the spectral position of the stop band. This simple example of the scaling laws of photonic crystals[56] allows one to tune the stop band across the photoluminescence spectrum of the dye. Bare (infiltrated) opals show a stop band minimum in the transmission spectrum at 500 (534), 560 (585), 588 (627), and 676 nm (730 nm) for microsphere diameters of 222, 240, 260, and 300 nm, respectively. Different shifts observed for opals having different l are likely due to the different overlap degree between the PC stop band and the bisTEG-PEPEP absorption band, which modifies the line shape of the spectra. The bathochromic shift of the stop band upon infiltration is due to the correspondent reduction of the dielectric contrast between the media composing the photonic crystal (water/polystyrene rather than air/polystyrene), as already quantitatively demonstrated in gold nanoparticle doped opals.[49–51] The same effect explains the observed reduction of the full width at half-maximum of the stop band upon infiltration.[49,50,57]

The energy position of the stop band (E_B) as well as its full width at half-maximum (ΔE_B) and their standard deviations are reported and compared in Table 1 for bare and infiltrated opals, as determined from reflectance and transmittance spectra. These data allow also one to calculate the Bragg length (L_B)

$$L_B = 2D\frac{E_B}{\pi \Delta E_B} \quad (1)$$

where D is the interplanar spacing in the [111] direction. L_B represents the attenuation per unit length of a transmitted wave in a photonic crystal for frequencies within the stop band. It is usually determined by measuring the transmitted light intensity attenuation in samples having different thicknesses.[14,58] A more sophisticated technique, coherent backscattering, provides more precise (almost 3 times) determination.[59] In our case, we can only use eq 1, being aware of its limits[60] but also of the reasonable optical quality of our bare opals testified by the reduced broadening in reflectance spectra. Indeed, for our opals $\Delta E_B/E_B = 0.06-0.07$ (see Table 1), while for so far mentioned papers its value is about 0.09. Notice also that for solution infiltrated opals $\Delta E_B/E_B$ is even further decreased (0.02−0.05). We also notice that, in all cases, $L_B < d$, thus indicating that light propagating inside the stop band is attenuated by coherent Bragg scattering (even though we cannot exclude a contribution from lambertian emission driven by defects). A confirmation that our opal films are thick enough to demonstrate fully developed photonic crystal properties can be obtained in the literature where it is demonstrated that, for about 20 layers of opals, the photonic properties are very close to those of a bulk sample.[3,61] Notice that our opals are more than 27 layers thick. All of these data indicate that our PhCs possess a suitable optical quality for the study we are performing.

The absorption spectrum of the dye in solution is also observed in spectra reported in Figure 3. The different intensities of this absorption for different opals are related to the different sample thicknesses.

An additional broad feature is observed at 440 nm for 300 nm bare opals. This is likely due to the same effect observed in bare opals and assigned to light diffraction along directions different from the (1,1,1) one. These features correspond to the excitation of photonic modes in the crystal having much higher energy than the stop band for low incidence angles.[48]

From the data shown in Figure 3, we observe that the degree of overlap between the stop band of infiltrated opals and the PL spectrum depends on the microsphere diameter. For 300 (222) nm opals, the stop band occurs in the low (high) energy tail of the PL spectrum. In contrast, very good overlap is obtained for 240 and 260 nm opals. However, since the stop band is expected to move toward higher energies by varying the collection angle, 260 nm opals allow for better matching the two spectra for all investigated angles. It should also be noted that for the 300 nm opal the stop band could overlap the PL spectrum only for very high collection angles, while for the 222 nm opal the overlap would be fully inhibited. However, we will show the importance of the study of emission spectra from all such opals in order to normalize the absolute value of the PL intensity (*vide infra*) and then to evaluate the presence of enhancement and suppression effects as a function of the emission angle.

Figure 4a shows the typical T spectra recorded at different incidence angle (θ) for a 260 nm opal infiltrated with a 1.4×10^{-3} M bisTEG-PEPEP water solution. The transmission dip associated with the stop band is observed at 627 nm at normal incidence and then shifts toward shorter wavelengths upon increasing θ. At about $\theta = 30°$, for this microsphere diameter, the stop band merges with the absorption of the dye, thus making the determination of its spectral position difficult. This effect depends on the dye concentration and cell thickness and can be more or less intense for different samples. Finally, it should be noted that the dye absorption is independent of the incidence angle, as expected. When more diluted solutions are used (3.5×10^{-4} M), the relative weight of the stop band is increased with respect to dye absorption, thus allowing the stop band dispersion to be better investigated (Figure 4b).

Dispersion properties of transmittance spectra have been measured for all cells prepared with opals having microspheres of different diameters and solutions of different concentrations. In Figure 4c, we report the typical dispersion of the stop band of such cells. For 300 nm opal cells, the stop band minimum can be easily recognized and even at the higher incidence angles

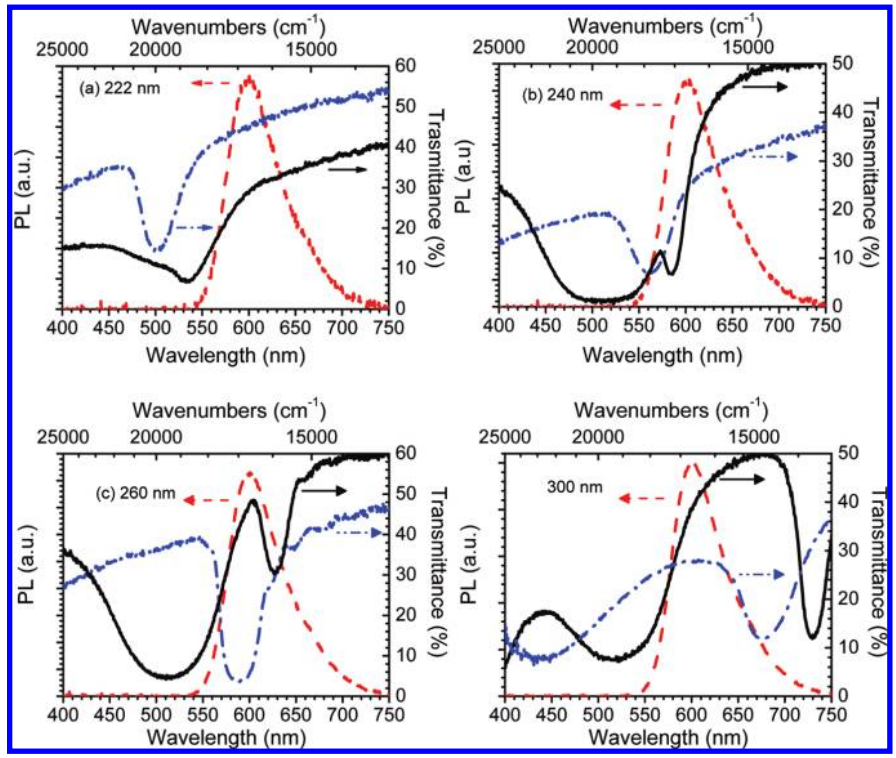

Figure 3. Transmittance spectra of bare (dash−dotted line), bisTEG-PEPEP solution infiltrated opal (full line), and bisTEG-PEPEP water solution PL spectra (dashed line). Microsphere diameter: 222 (a), 240 (b), 260 (c), and 300 (d) nm.

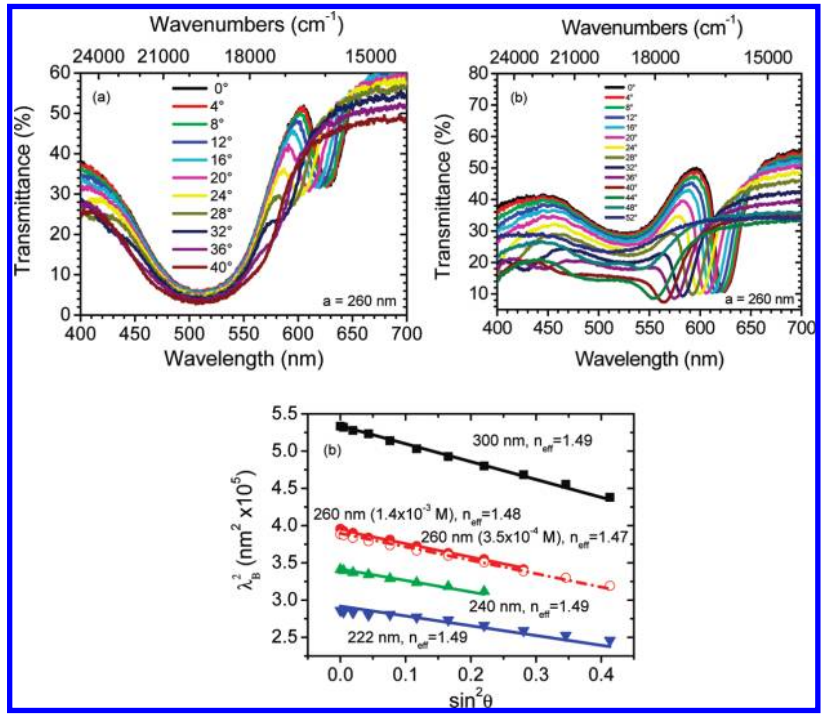

Figure 4. Angular dispersion of transmittance spectra for opals (a = 260 nm) infiltrated with bisTEG-PEPEP water solutions of different concentrations: (a) 1.4×10^{-3} M; (b) 3.5×10^{-4} M. (c) Stop band minimum vs incidence angle for infiltrated opals made with microspheres having different diameters. Lines are Bragg−Snell law fits.

does not overlap with dye absorption. For other diameters, this effect, as noticed before, is more or less remarkable and weakly affects the dispersion properties. For 222 nm opal cells, the stop band is high energy detuned from the strong dye absorption spectrum and then, again, the dispersion can be investigated in a wide range of angles.

In general, dispersion data can be easily fitted with the Bragg−Snell law:[27,57,62–65]

$$m\lambda_B = 2D\sqrt{n_{eff}^2 - \sin^2\theta} \quad (2)$$

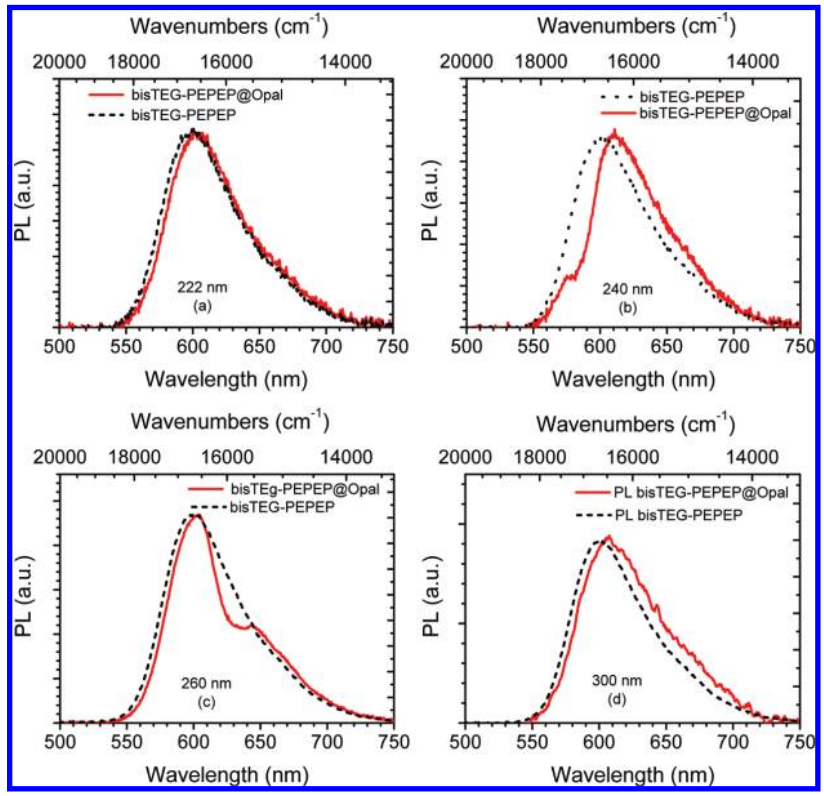

Figure 5. Comparison of peak normalized photoluminescence spectra of free bisTEG-PEPEP solution and infiltrated in opals ($\theta' = 0$) made with microspheres of different diameters: (a) 222, (b) 240, (c) 260, and (d) 300 nm.

where m is the diffraction order, $\lambda_B = hc/E_B$, and n_{eff} the effective refractive index of solution infiltrated opals. By fixing the value of $D = a(2/3)^{0.5}$ with the nominal one assuming a face centered cubic (FCC) compact structure, we get $n_{eff} = 1.47-1.49$ (Figure 5c, lines). For bare opals, we usually found $n_{eff} \approx 1.40$, to be compared to the theoretical one predicted with the effective medium theory $n_{eff} \approx 1.41$.

The value of n_{eff} determined from the dispersion of transmittance spectra is important to obtain a reasonable estimate of the dielectric constant (ε_i) or refractive index (n_i) of interstices. As a matter of fact, it has been recently shown for opals doped with gold nanoparticles[49–51,66] that n_{eff} is connected to n_i by the Lorentz−Lorenz formula for the effective medium

$$\frac{\varepsilon_{eff} - 1}{\varepsilon_{eff} + 2} = f_{PS}\frac{\varepsilon_{PS} - 1}{\varepsilon_{PS} + 2} + (1 - f_{PS})\frac{\varepsilon_i - 1}{\varepsilon_i + 2} \qquad (3)$$

where $\varepsilon_{eff} = (n_{eff})^2$, $\varepsilon_{PS} = 2.53$ is the dielectric constant of the polystyrene sphere, ε_i is the dielectric constant of the interstices ($\varepsilon_i = 1$ for bare opals), and f_{PS} is the volume fraction of the unitary cell filled with nanospheres (0.74 for a close packed FCC crystal). By inverting eq 3, we obtain $\varepsilon_i = 1.35/1.50$ (or $n_i = 1.16/1.23$) for input values $\varepsilon_{eff} = 2.16/2.22$ ($n_{eff} = 1.47/1.49$) as previously derived from the Bragg−Snell fit. The minor uncertainty of n_{eff} values derived from experimental data implies a remarkable uncertainty in ε_i (n_i). Moreover, since water was used as a solvent, we expected a value for n_i very close to 1.33, the refractive index of water. The lower value of n_i here deduced would in principle mean that imperfect infiltration occurred. However, we noticed that the standard deviation of microsphere diameter is 5%, thus inducing a correspondent variation of the stop band spectral position and then affecting the results of the Bragg−Snell fit. As a matter of fact, by fitting data reported in Figure 4c for 300 nm opals by assuming $a = 300 \pm 7.5$ nm ($\pm 2.5\%$ times a, the standard deviation provided by the microsphere producer), we found $n_{eff} = 1.46/1.53$. This n_{eff} values correspond from eq 3 to $\varepsilon_i = 1.28/1.86$ ($n_i = 1.13/1.37$), i.e., a dielectric constant of the interstices significantly more spread than corresponding values found from the Bragg−Snell fit obtained by setting the nominal sphere diameter ($a = 300$ nm). This example demonstrate that uncertainty of n_{eff} (and then n_i) is due to the uncertainty in the determination of the sphere diameter.

Figure 5 shows the peak normalized PL spectra of bisTEG-PEPEP solutions compared with those of the same solution infiltrated in opals with $a = 222$ (a), 240 (b), 260 (c), and 300 (d) nm and recorded at the detection angle $\theta' = 0$. As already observed for the data of Figure 3, the spectral position of the opal stop band depends on microsphere diameter. For $a = 222$ nm opals (Figure 5a), the PL spectra are almost indistinguishable, since the stop band is around 500 nm and then it does not overlap the PL spectrum. For $a = 240$ nm opals, the stop band is at 580 nm and its evidence in the PL spectrum is a modification of its high energy tail. For $a = 260$ nm opals, a clear dip in the PL spectrum is observed at 630 nm due to good overlap with the stop band spectral region. The photonic crystal stop band acts as a filter and prevents the light of specific frequencies to escape from the infiltrated opal in specific directions.[16,67] This is a general feature of photonic crystals due to the redistribution of the density of photonic states in the k-space, which in some cases could lead to a modification of the probability of spontaneous emission, thus affecting the radiative lifetime.[16,17,21,22] However, it is worth noticing that, in low dielectric-contrast photonic crystals, such as those discussed in this work, variations in the radiative lifetime are expected to be typically very small. Finally, for $a = 300$ nm opals, since the stop band is overlapped to the low energy tail of the PL

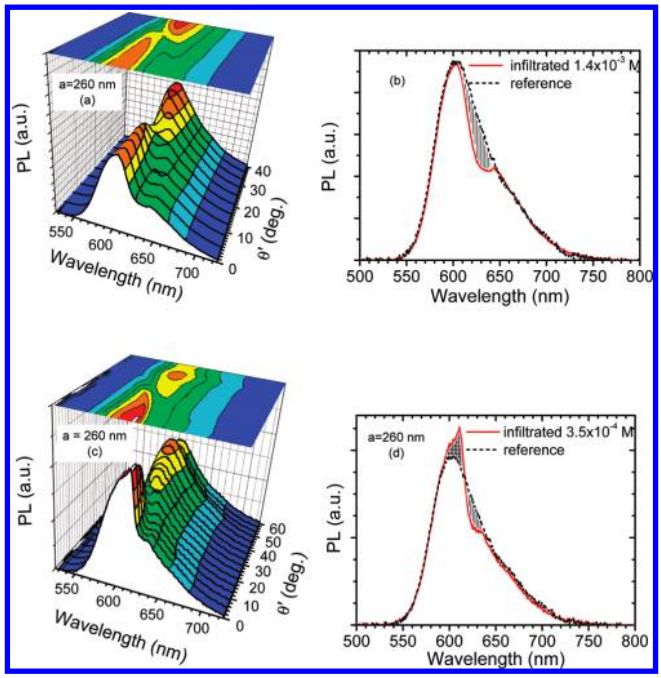

Figure 6. Detection angle (θ') dependence of PL spectra of bisTEG-PEPEP solutions infiltrated in 260 nm opals (a and b, 1.4×10^{-3} M; c and d, 3.5×10^{-4} M). Comparison of $\theta' = 0$ PL spectra for parts a and c (b and d, respectively; full line) with the reference spectra (dotted line). The vertical (crossed) dashed area indicates s filtering (enhancing) effects.

spectrum (~730 nm) where the signal is very weak, no evident effects are observed. For all spectra, an apparent modification of the intensity of the low or high energy tail is observed. This is due to the adopted normalization procedure (peak normalization) and should not be confused with modification of light emission, implying possible enhancement/suppression effects due to the presence of the photonic crystal. This item will be discussed later on in detail.

As already mentioned, $a = 260$ nm opals show the better overlap between stop band and bisTEG-PEPEP emission. The dispersion properties of PL spectra as a function of the detection angle for opals infiltrated with solutions of different concentration are depicted in Figure 6. By changing θ', the filtering effect, i.e., the minimum in the PL spectrum shifts toward lower wavelengths according to the PhC dispersion properties and deeply modifies the spectrum. Around $\theta' = 24°$, a double peak structure appears, and by further increasing the detection angle, the stop band reduces the signal in the high energy tail of the PL spectrum in a manner similar to that previously observed for $a = 240$ nm opals (Figure 5b). The crossing of the stop band over the PL spectrum upon changing θ' can be more easily observed in the contour plot over Figure 6a where the projection of the PL spectra is reported with a color code associated with PL intensity. Notice that the dispersion of the minimum in the PL spectrum provided a value $n_{\text{eff}} = 1.49$ very similar to that previously observed for the stop band in transmission spectra (Figure 4b), thus confirming the common origin of the spectral features observed in the two measurements.

The results so far reported are very important for different reasons. First of all, they demonstrated that we succeeded in the infiltration of opals with a solution of bisTEG-PEPEP, a new ad hoc synthesized chromophore with enhanced nonlinear optical properties. Moreover, in spite of the reduced dielectric contrast between polystyrene microspheres and bisTEG-PEPEP water solutions, the photonic stop band can still be clearly observed. This is a prerequisite to any further investigation on these systems. Finally, the filtering effect of the stop band on the PL spectrum is clearly observed, thus demonstrating that the investigation of emission properties of an ad hoc synthesized quadrupolar dye solution infiltrating opals is possible.

Possible enhancement and suppression effects due to a redistribution of the photonic density of states in opals, which imply a modification of PL emission intensity along specific directions, are now discussed. It is known that at the high (low) energy edges of the stop band the electromagnetic field is confined in the low (high) dielectric constant material composing the photonic crystal.[56] In particular, for those photon energies, the field is not propagating but behaves as a stationary wave being confined in the interstices (microspheres). This effect has been recently shown to modify the T spectrum of opals doped with gold nanoparticles when the stop band is tuned over the broad aggregated nanoparticle absorption.[50] Even in PL spectra of emitter infiltrated opals, anomalous lineshapes and radiative decay modifications associated with light localization or other effects due to the photonic crystal band structure have been reported.[14–17,20–22,27,28,68–70] In order to evaluate the angular-dependent enhancement effects of PL, a detailed comparison of the *absolute* PL intensity of emitter inside and outside the photonic crystal must be performed. This nontrivial problem concerns light extraction from the cell and light collection by the optical setup and has also been widely investigated in different frameworks like improving organic light emitting diode performances,[71] correcting anisotropic refractive and self-absorption effects on PL spectra of oriented conjugated polymers,[72] and favoring light insertion in photovoltaic cells.[73] In the case of emission from photonic crystals, proper normalization procedures have been adopted. The simpler reference could be the free solution used for infiltration filled in a cell having the same thickness of the opal. However, the light extraction efficiency of these cells is 1.5−8 times less efficient than that for solution infiltrated opals as measured over several cells of different thicknesses. This indicates that more complicated approaches have to be used to solve the problem. For instance, Barth et al.[21] compared the intensity of emission from rhodamine B infiltrated opals obtained from ordered and disordered regions of the same opal and then they normalized their intensity to the low energy tail of such spectra. Since spectra from ordered regions have a fingerprint of the stop band while disordered regions do not, this approach allows for an absolute value comparison. Lodhal[22] and Bechger[20] used as a reference the PL spectrum obtained by the same sample recorded at very high values of θ' such as no stop band appears in the PL spectrum. In this case too, long wavelength normalization of the spectra was adopted.

In this work, we used a similar approach to normalize the intensity of our spectra (namely, PL spectra recorded for opals with stop band fully detuned from it, both at high and low energies, or normalized with spectra recorded at $\theta' = 60°$ from the same sample) and results will be compared and discussed. For what concerning data in Figure 6, we used the spectra recorded at $\theta' = 60°$ (i.e., when the stop band is detuned from the PL spectrum) as a reference for comparison with the spectra of the same sample recorded at $\theta' = 0°$. Spectra reported in Figure 6b showed only the filtering effect of the stop band on the PL spectrum (~640 nm, dashed area) but no PL enhancement was observed for any emission direction, conversely from what was reported in refs 20–22. This result cannot be understood when considering the good optical quality of our opals. For this reason, we repeated the experiments with more

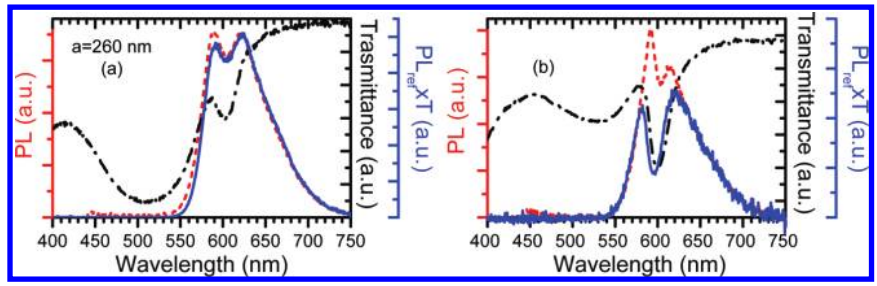

Figure 7. Comparison of T (dashed−dotted line) and PL (dashed line) spectra at $\theta = 0°$ for 260 nm opals infiltrated with 1.4×10^{-3} (a) and 3.5×10^{-4} (b) solutions and the calculated spectrum obtained by multiplying T with PL_{ref} (full line).

diluted solutions (3.5×10^{-4} M). Transmittance spectra of opals infiltrated with the new solutions (Figure 4b) show a more pronounced stop band relative to previous samples (Figure 4a). Since the stop band can be easily detected for large incidence angles without being too much masked by absorption, a more extended dispersion range can be used for Bragg−Snell fit (Figure 4c), providing $n_{eff} = 1.47$. Figure 6c shows the dispersion properties of PL spectra of these new opals, which are comparable to previous ones ($n_{eff} = 1.48$). However, a detailed comparison of PL spectra recorded for $\theta' = 0$ with the reference (Figure 6d) clearly shows enhancement effects in the 590−620 nm region (crossed dashed area). In addition, a stop band filtering effect is also observed (~640 nm, vertical dashed area), even though it is less pronounced than in the previous case. These results demonstrate the importance of avoiding PL self-absorption in order to observe the effect of the photonic band structure on the emission properties.

An additional support of the different photon−matter interaction in the opals infiltrated with the two solutions is reported in Figure 7. There, the $\theta' = 0°$ PL spectra of opals infiltrated with concentrated (a) and diluted (b) bisTEG-PEPEP water solutions are compared with the reference PL spectra (PL_{ref}) multiplied by the correspondent T ones (also reported in Figure 7 for comparison). For concentrated solutions, the $PL_{ref} \times T$ spectrum is almost identical to the measured PL one, thus indicating that the PC plays the role of a bare filter. On the contrary, for opals infiltrated with diluted solutions, the PL spectrum is noticeably different than $PL_{ref} \times T$ even in correspondence of the photonic stop band. Notice also that the stop band in T spectra causes a minimum at 600 nm while in PL ones the minimum is observed at 605 nm and in $PL_{ref} \times T$ at 595 nm. These meaningful differences are an additional indication of the sophisticated effect of light−matter interaction occurring in this sample which is not only related to the simple stop band filtering action. Even more evident is the different intensity of the spectra. The intensity of the PL spectrum from the opal is noticeably larger than that calculated for $PL_{ref} \times T$, indicating the existence of enhancement effects. In order to better highlight the enhancement effects and to take into account their angular dependence, the dispersion properties are analyzed in closer detail in Figure 8 where we report and compare the transmission dispersion properties (Figure 8a) of opals infiltrated with diluted solutions and the PL spectra from 260 nm opals divided by the different PL references previously indicated, namely, opals having $a =$ 222 nm (Figure 8b, stop band high energy detuned), $a = 260$ nm $\theta' = 60°$ (Figure 8c, internal reference with stop band high energy detuned), $a = 300$ nm (Figure 8d, stop band low energy detuned). All measurements are recorded for the same detection angles. We would like to remember that these ratio spectra are normalized to unit at low photon energies as usually reported in the literature.[20–22] This correction affects the ratio spectra for an amount below 10% of the value at long wavelength.

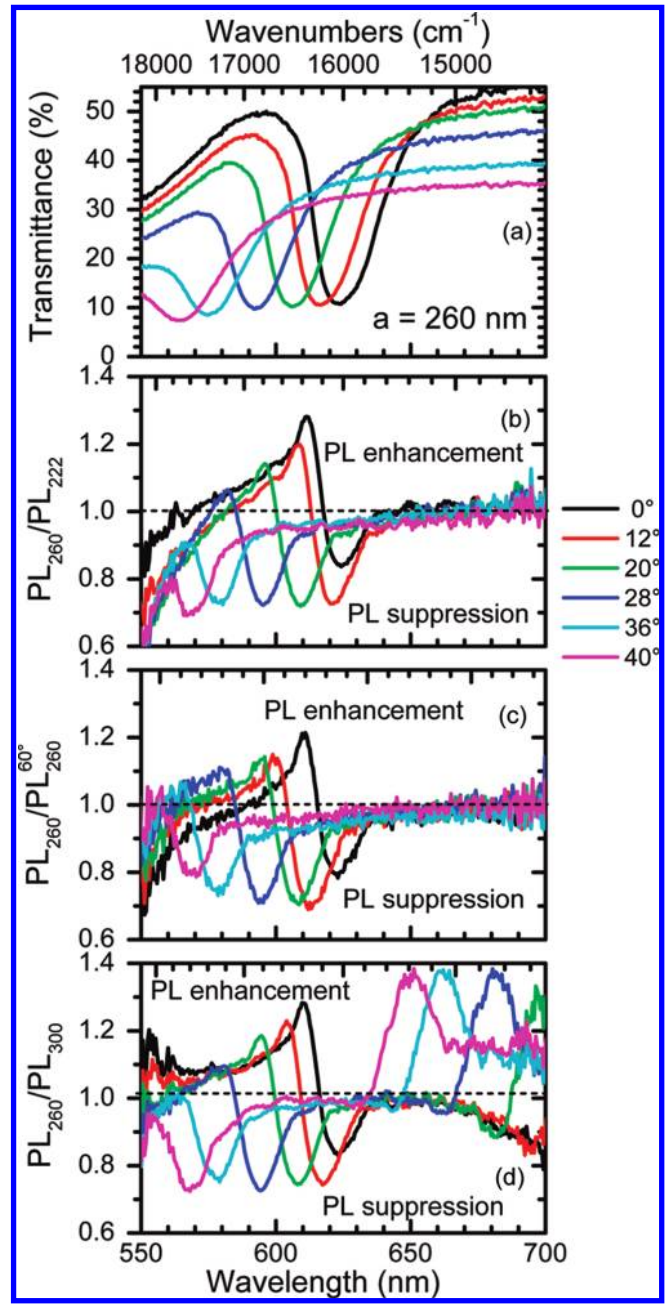

Figure 8. Dispersion properties of 260 nm opals infiltrated with bisTEG-PEPEP solutions. (a) Transmission spectra. PL ratio spectra calculated with different references: (b) 222 nm opal; (c) 260 nm opal at $\theta' = 60°$; (c) 300 nm opal.

Ratio spectra in Figure 8 show, at each specific angle, a PL intensity enhancement for ratios larger than 1 and a PL suppression when ratios are lower than 1. For the wavelengths larger than 630 nm, ratios are equal to 1, indicating that no

enhancement or suppression is observed. An exception occurs for 300 nm opals (data in Figure 8c), since in that case the stop band of the reference is long wavelength detuned with respect to the emission and an apparent enhancement is observed due to the low energy position of the stop band in the reference spectra for this particular reference. Within the stop band, for all references, the ratio is lower than 1 (PL reduction) due to the stop band filtering effect already pointed out. Noticeably, directional enhancement and suppression effects are observed in the high energy edge of the stop band and over a wide angular range, independently of the reference used. The spectral coincidence of the enhancement and suppression regions with the high energy stop band edge and with the center of the stop band respectively give a strong indication that modification of light emission is occurring due to a redistribution of the photonic density of states in the *k*-space. This result is in full agreement with previous findings indicating that dye molecules are within the interstices.[20,21] It is important to stress at this point that a modification of the photonic density of states could lead to an enhancement or a suppression of emission at *specific* wavelengths and along *specific* directions. However, this does not necessarily lead to an overall enhancement or suppression of the emission rate, i.e., an increase or a decrease of the radiative lifetime of an emitter placed inside the photonic crystal. Indeed, a sizable modification of the radiative lifetime (Purcell effect[74]) can only be observed in photonic crystals for which the photonic density of states is strongly modified in the whole *k*-space, i.e., for any propagation direction. Thus, in the case of infiltrated direct opals which show a substantial modification of the photonic density of states only for particular *k*-values, directional enhancement or suppression of emission could be considerable, while effects on the radiative lifetime are usually very small and hard to detect.

From the theory,[56] enhancement of emission is expected in both sides of the photonic stop band. Barth et al.[21] showed PL enhancement also for the low energy stop band edge, an occurrence caused by molecules located at the contact point between opal microspheres. Data in Figure 8 do not show such an effect, but a tentative indication of that could be traced back to the reduced stop band filtering effect in PL spectra in the low energy side of the stop band edge (see Figure 7b). Dishomogeneous distribution of dye molecules within the interstices among spheres due to capillary forces can contribute to modifying enhancement effects at high and low energy stop band edges.[21] Indeed, at the high energy edge, molecules facing the voids between beds do not contribute.[21] At the low energy pseudogap edge, the situation is more complicated: molecules from bed contact points provide a reduction of the density of states while molecules facing voids give an enhancement. Then, at the low energy side, the two contributions seem to almost cancel each other out. We also notice that the light localization effect at the high energy stop band edge implies a confinement into the low dielectric constant material, i.e., the solution where the emitter is dispersed, thus making this enhancement more efficient with respect to that at the low energy edge, which corresponds to localization within PS microspheres. It is interesting to notice that in spite of the low dielectric contrast between PS microspheres and the interstices filled with the bisTEG-PEPEP solution, i.e., the active material, the enhancement and suppression effect along specific directions is clearly observed. In order to assess a possible overall emission enhancement and an increase of the radiative rate, one should perform time-resolved PL experiments on the infiltrated opals, although little effects on the emission lifetime are expected in this case.[21,27]

An alternative explanation to similar experimental data has been provided by Nikolaev et al.[28] By considering that light emitted inside the PhC could be both lambertian-like diffused by defects as well as directionally diffracted by the photonic crystal planes, they calculated the effect of internal reflection losses at the interface during light way out from the opal. Their calculations applied to opal and inverse opals of different dielectric contrast showed that enhancement of emission at the edges of the stop band can be reproduced by simple optical effects without invoking an increase of the local density of photonic states or modification of the radiative transition rate. Even though in our case a minor contribution from lambertian emission due to defects cannot be excluded, a certain difference with the Nikolaev et al. results does exist. Indeed, their calculations show that the enhancement can be observed at the high energy side of the stop band for detection angles below 30° while in the low energy side for higher θ'. This result is in contrast with our data where the enhancement is observed (for every reference) only in the high energy stop band side independently for all investigated detection angles. A definitive discrimination between the two models is very difficult, since an isotropical dye distribution is assumed by Nikolaev et al.[28] while Barth et al. pointed out the importance of dye position inside interstices.[21] Moreover, in our case, the situation is even more complicated, since a lower dielectric contrast is present. In principle, only the study of the PL dynamics could disentangle the situation being the inhibition of the radiative decay associated only to the DOS redistribution model. In this case, PL decays for free or PhC infiltrated dyes would be very different. Unfortunately, even such studies have not so far allowed a generalized consensus on these topics to be achieved (see ref 27 and references therein).

Due to the uncertainties so far described and the availability of steady-state data here reported, we feel that probably both mechanisms might be active in bisTEG-PEPEP infiltrated opals, but a clear disentanglement between their relative importance is very difficult. This opens new perspectives to the study of the photophysics of PhC infiltrated with chemically engineered photoactive conjugated materials (possibly in the solid state).

Conclusions

In conclusion, we showed that multipolar chromophores possessing a large two-photon absorption cross section can be efficiently functionalized with hydrophilic chains in order to promote their solubility in polar solvent. This property allowed to succeed in the infiltration of polystyrene artificial opals of good optical quality. The infiltration process induces a red shift of the photonic stop band as well as a reduction of its width. Even though the dielectric properties of the infiltrated photonic crystals result to be modified, the residual dielectric contrast is strong enough to modulate the emission properties of the chromophore inside the interstices.

When chromophores are photoexcited, they emit light filtered by the opal for photon energies tuned over the stop band spectral range. For high quality opals infiltrated with properly diluted solutions, remarkable PL directional enhancement effects at the high energy stop band edges are observed due to redistribution of the PC density of photonic states. However, we cannot exclude that internal reflection losses might contribute to the observed effect.

We hope these results might stimulate further investigations on the exploitation of the large nonlinear optical properties of

bisTEG-PEPEP dyes and chemically engineered conjugated molecules when used in the field of PhC, in particular for optical limiting, up-conversion lasing, and fluorescence applications.

Acknowledgment. We gratefully acknowledge financial support from the Italian Ministry of University and Research through programs MIUR-PRIN 2006031511 and MIUR-FIRB RBNE033KMA.

Supporting Information Available: Optical setup used for variable angle transmittance and photoluminescence spectroscopy. This material is available free of charge via the Internet at http://pubs.acs.org.

References and Notes

(1) John, S. *Phys. Rev. Lett.* **1987**, *58*, 2486.
(2) Yablonovitch, E. *Phys. Rev. Lett.* **1987**, *58*, 2059.
(3) Galisteo-Lopez, J. F.; Palacios-Lidon, E.; Castillo-Martinez, E.; Lopez, C. *Phys. Rev. B* **2003**, *68*, 115109.
(4) Blanco, A.; Chomski, E.; Grabtchak, S.; Ibisate, M.; John, S.; Leonard, S. W.; Lopez, C.; Meseguer, F.; Minguez, H.; Mondia, J. P.; Ozin, G. A.; Toader, O.; Driel, H. M. v. *Nature* **2000**, *405*, 437.
(5) DiStasio, F.; Berti, L.; Burger, M.; Marabelli, F.; Gardin, S.; Dainese, T.; Signorini, R.; Bozio, R.; Comoretto, D. *Phys. Chem. Chem. Phys.* **2009**, *11*, 11310.
(6) Lopez, C. *Adv. Mater.* **2003**, *15*, 1679.
(7) Markowicz, P.; Friend, C.; Shen, Y.; Swiatkiewicz, J.; Prasad, P. N.; Toader, O.; John, S.; Boyd, R. W. *Opt. Lett.* **2002**, *27*, 351.
(8) Markowicz, P. P.; Tiryaki, H.; Pudavar, H.; Prasad, P. N.; Lepeshkin, N. N.; Boyd, R. W. *Phys. Rev. Lett.* **2004**, *92*, 83903.
(9) Polson, R. C.; Chipouline, A.; Vardeny, Z. V. *Adv. Mater.* **2001**, *13*, 760.
(10) Shkunov, M. N.; Vardeny, Z. V.; DeLong, M. C.; Polson, R. C.; Zakhidov, A. A.; Baughman, R. H. *Adv. Funct. Mater.* **2002**, *12*, 21.
(11) Eradat, N.; Sivachenko, A. Y.; Raikh, M. E.; Vardeny, Z. V.; Zakhidov, A. A.; Baughman, R. H. *Appl. Phys. Lett.* **2002**, *80*, 3491.
(12) Sumioka, K.; Nagahama, H.; Tsutsui, T. *Appl. Phys. Lett.* **2001**, *78*, 1328.
(13) Kolaric, B.; Baert, K.; Van der Auweraer, M.; Vallee, R. A. L.; Clays, K. *Chem. Mater.* **2007**, *19*, 5547.
(14) Romanov, S. G.; Maka, T.; Torres, C. M. S.; Muller, M.; Zentel, R. *J. Appl. Phys.* **2002**, *91*, 9426.
(15) Solovyev, V. G.; Romanov, S. G.; Chigrin, D. N.; Sotomayor Torres, C. M. *Synth. Met.* **2003**, *139*, 601.
(16) Petrov, E. P.; Bogomolov, V. N.; Kalosha, I. I.; Gaponenko, S. V. *Phys. Rev. Lett.* **1998**, *81*, 77.
(17) Koenderink, A. F.; Vos, W. L. *Phys. Rev. Lett.* **2003**, *91*, 213902.
(18) Noh, H.; Scharrer, M.; Anderson, M. A.; Chang, R. P. H.; Cao, H. *Phys. Rev. B* **2008**, *77*, 115136.
(19) Yu, A. V.; Luterova, K.; Pelant, I.; Honerlage, B.; Astratov, V. N. *Appl. Phys. Lett.* **1997**, *71*, 1616.
(20) Bechger, L.; Lodahl, P.; Vos, W. L. *J. Phys. Chem. B* **2005**, *109*, 9980.
(21) Barth, M.; Gruber, A.; Cichos, F. *Phys. Rev. B* **2005**, *72*, 085129.
(22) Lodhal, P.; vanDriel, A. F.; Nikolaev, I. S.; Irman, A.; Overgaag, K.; Vanmaekelbergh, D.; Vos, W. L. *Nature* **2004**, *430*, 654.
(23) Deutsch, M.; Vlasov, Y. A.; Norris, D. J. *Adv. Mater.* **2000**, *12*, 1176.
(24) Kurbanov, S. S.; Shaymardanov, Z. S.; Kasymdzhanov, M. A.; Khabibullaev, P. K.; Kang, T. W. *Opt. Mater.* **2007**, *29*, 1177.
(25) Eradat, N.; Wohlgenannt, M.; Vardeny, Z. V.; Zakhidov, A. A.; Baughman, R. H. *Synth. Met.* **2001**, *116*, 509.
(26) Nikolaev, I. S.; Lodahl, P.; Vos, W. L. *J. Phys. Chem. C* **2008**, *112*, 7250.
(27) Kubo, S.; Fujishima, A.; Sato, O.; Segawa, H. *J. Phys. Chem. C* **2009**, *113*, 11704.
(28) Nikolaev, I. S.; Lodahl, P.; Vos, W. L. *Phys. Rev. A* **2005**, *71*, 053813.
(29) Abbotto, A.; Beverina, L.; Bozio, R.; Facchetti, A.; Ferrante, C.; Pagani, G. A.; Pedron, D.; Signorini, R. *Org. Lett.* **2002**, *4*, 1495.
(30) For a recent review, see: He, G. S.; Tan, L.-S.; Zheng, Q.; Prasad, P. N. *Chem. Rev.* **2008**, *108*, 1245.
(31) Kim, H. M.; Jeong, B. H.; Hyon, J.-Y.; An, M. J.; Seo, M. S.; Hong, J. H.; Lee, K. J.; Kim, C. H.; Joo, T.; Hong, S.-C.; Cho, B. R. *J. Am. Chem. Soc.* **2008**, *130*, 4246.
(32) Picot, A.; D'Aleo, A.; Baldeck, P. L.; Grichine, A.; Duperray, A.; Andraud, C.; Maury, O. *J. Am. Chem. Soc.* **2008**, *130*, 1532.
(33) Krishna, T. R.; Parent, M.; Werts, M. H. V.; Moreaux, L.; Gmouh, S.; Charpak, S.; Caminade, A.-M.; Majoral, J.-P.; Blanchard-Desce, M. *Angew. Chem., Int. Ed.* **2006**, *45*, 4645.
(34) Mohan, P. S.; Lim, C. S.; Tian, Y. S.; Roh, W. Y.; Lee, J. H.; Cho, B. R. *Chem. Commun.* **2009**, *36*, 5365.
(35) Boca, S. C.; Four, M.; Bonne, A.; Sanden, B.v.d.; Astilean, S.; Baldeck, P. L.; Lemercier, G. *Chem. Commun.* **2009**, *30*, 4590.
(36) Beverina, L.; Crippa, M.; Landenna, M.; Ruffo, R.; Salice, P.; Silvestri, F.; Versari, S.; Villa, A.; Ciaffoni, L.; Collini, E.; Ferrante, C.; Bradamante, S.; Mari, C. M.; Bozio, R.; Pagani, G. A. *J. Am. Chem. Soc.* **2008**, *130*, 1894.
(37) Belfield, K. D.; Bondar, M. V.; Hernandez, F. E.; Masunov, A. E.; Mikhailov, I. A.; Morales, A. R.; Przhonska, O. V.; Yao, S. *J. Phys. Chem. C* **2009**, *113*, 4706.
(38) Zheng, Q.; Gupta, S. K.; He, G. S.; Tan, L.-S.; Prasad, P. N. *Adv. Funct. Mater.* **2008**, *18*, 2770.
(39) Signorini, R.; Pedron, D.; Ferrante, C.; Bozio, R.; Brusatin, G.; Innocenzi, P.; Della Negra, F.; Maggini, M.; Abbotto, A.; Beverina, L.; Pagani, G. A. *SPIE Proc.* **2003**, *4797*, 1.
(40) Belfield, K. D.; Liu, Y.; Negres, R. A.; Fan, M.; Pan, G.; Hagan, D. J.; Hernandez, F. E. *Chem. Mater.* **2002**, *14*, 3663.
(41) O'Connor, N. A.; Berro, A. J.; Lancaster, J. R.; Gu, X.; Jockusch, S.; Nagai, T.; Ogata, T.; Lee, S.; Zimmerman, P.; Willson, C. G.; Turro, N. J. *Chem. Mater.* **2008**, *20*, 7374.
(42) Bouit, P.-A.; Kamada, K.; Feneyrou, P.; Berginc, G.; Toupet, L.; Maury, O.; Andraud, C. *Adv. Mater.* **2009**, *21*, 1151.
(43) Tsiminis, G.; Ribierre, J.-C.; Ruseckas, A.; Barcena, H. S.; Richards, G. J.; Turnbull, G. A.; Burn, P. L.; Samuel, I. D. W. *Adv. Mater.* **2008**, *20*, 1940.
(44) Abbotto, A.; Beverina, L.; Bozio, R.; Bradamante, S.; Ferrante, C.; Pagani, G. A.; Signorini, R. *Adv. Mater.* **2000**, *12*, 1963.
(45) Pasternack, R. F.; Fleming, C.; Herring, S.; Collins, P. J.; dePaula, J.; DeCastro, G.; Gibbs, E. J. *Biophys. J.* **2000**, *79*, 550.
(46) Signorini, R.; Ferrante, C.; Pedron, D.; Zerbetto, N.; Cecchetto, E.; Slaviero, N.; Fortunati, I.; Collini, E.; Bozio, R.; Abbotto, A.; Beverina, L.; Pagani, G. A. *J. Phys. Chem. A* **2008**, *112*, 4224.
(47) Cucini, M.; Comoretto, D.; Galli, M.; Marabelli, F.; Abbotto, A.; Bellotto, L.; Marinzi, C. *SPIE Proc.* **2008**, *6999*, 69992D.
(48) Pavarini, E.; Andreani, L. C.; Soci, C.; Galli, M.; Marabelli, F.; Comoretto, D. *Phys. Rev. B* **2005**, *72*, 045102.
(49) Morandi, V.; Marabelli, F.; Amendola, V.; Meneghetti, M.; Comoretto, D. *Adv. Funct. Mater.* **2007**, *17*, 2770.
(50) Morandi, V.; Marabelli, F.; Amendola, V.; Meneghetti, M.; Comoretto, D. *J. Phys. Chem. C* **2008**, *112*, 6293.
(51) Comoretto, D.; Morandi, V.; Marabelli, F.; Amendola, V.; Meneghetti, M. *SPIE Proc.* **2006**, *6182*, 61820D.
(52) Comoretto, D.; Grassi, R.; Marabelli, F.; Andreani, L. C. *Mater. Sci. Eng., C* **2003**, *23*, 61.
(53) Abbotto, A.; Beverina, L.; Pagani, G. A.; Collini, M.; Chirico, G.; D'Alfonso, L.; Baldini, G. *SPIE Proc.* **2003**, *5139*, 223.
(54) Facchetti, A.; Beverina, L.; Boom, M. E. V. d.; Dutta, P.; Evmenenko, G.; Shukla, A. D.; Stern, C. E.; Pagani, G. A.; Marks, T. J. *J. Am. Chem. Soc.* **2006**, *128*, 2142.
(55) Lottner, C.; Bart, K.-C.; Bernhardt, G.; Brunner, H. *J. Med. Chem.* **2002**, *45*, 2079.
(56) Joannopulos, J. D.; Meade, R. D.; Win, J. N. *Photonic Crystals: Molding the Flow of the Light*; Princeton University Press: Princeton, NJ, 1995.
(57) Vos, W. L.; Sprik, R.; Blaaderen, A.v.; Imhof, A.; Lagendijk, A.; Wegdam, G. H. *Phys. Rev. B* **1996**, *53*, 16231.
(58) Vlasov, Y. A.; Astratov, V. N.; Baryshev, A. V.; Kaplyanskii, A. A.; Karimov, O. Z.; Limonov, M. F. *Phys. Rev. E* **2000**, *61*, 5784.
(59) Huang, J.; Eradat, N.; Raikh, M. E.; Vardeny, Z. V.; Zakhidov, A. A.; Baughman, R. H. *Phys. Rev. Lett.* **2001**, *86*, 4815.
(60) Vlasov, Y. A.; Deutsch, M.; Norris, D. J. *Appl. Phys. Lett.* **2000**, *76*, 1627.
(61) Galisteo-Lopez, J. F.; Galli, M.; Patrini, M.; Balestreri, A.; Andreani, L. C.; Lopez, C. *Phys. Rev. B* **2006**, *73*, 125103.
(62) Astratov, V. N.; Vlasov, Y. A.; Karimov, O. Z.; Kaplyanskii, A. A.; Musikhin, Y. G.; Bert, N. A.; Bogomolov, V. N.; Prokofiev, A. V. *Phys. Lett. A* **1996**, *222*, 349.
(63) Park, S. H.; Xia, Y. *Langmuir* **1999**, *15*, 266.
(64) Reynolds, A.; Lopez-Tejeira, F.; Cassagne, D.; Garcia-Vidal, F. J.; Jouanin, C.; Sanchez-Dehesa, J. *Phys. Rev. B* **1999**, *60*, 11422.
(65) Miclea, P. T.; Susha, A. S.; Liang, Z.; Caruso, F.; Sotomayor-Torres, C. M.; Romanov, S. G. *Appl. Phys. Lett.* **2004**, *84*, 3960.
(66) Cucini, M.; Alloisio, M.; Demartini, A.; Comoretto, D. *Biomimetic and Supramolecular Systems Research*; Nova Science Publishers Inc.: Hauppauge, NY, 2008.
(67) Megens, M.; Wijnhoven, J. E. G. J.; Lagendijk, A.; Vos, W. L. *J. Opt. Soc. Am. B* **1999**, *2*, 1.

(68) Bulu, I.; Caglayan, H.; Ozbay, E. *Phys. Rev. B* **2003**, *67*, 205103.
(69) Vlasov, Y. A.; Luterova, K.; Pelant, I.; Honerlage, B.; Astratov, V. N. *Appl. Phys. Lett.* **1997**, *71*, 1616.
(70) Zhang, Y.-Q.; Wang, J.-X.; Ji, Z.-Y.; Hu, W.-P.; Jiang, L.; Song, Y.-L.; Zhu, D.-B. *J. Mater. Chem.* **2007**, *17*, 90.
(71) Wan, W. M. V.; Greenham, N. C.; Friend, R. H. *J. Appl. Phys.* **2000**, *87*, 2542.
(72) Soci, C.; Comoretto, D.; Marabelli, F.; Moses, D. *Phys. Rev. B* **2007**, *75*, 075204.
(73) *Organic Photovoltaics*; Brabec, C., Dyakonov, V., Parisi, J., Sariciftci, N. S. Eds.; Springer-Verlag: Berlin, Heidelberg, 2003; Vol. 60.
(74) Purcell, E. M. *Phys. Rev. B* **1946**, *69*, 681.

JP906002Q